Stereoelectronic Properties of Photosynthetic and Related Systems. 2. Ab Initio Quantum Mechanical Ground State Characterization of Magnesium Porphine, Magnesium Chlorin, and Ethyl Chlorophyllide *a*

Dale Spangler,[1,2] Gerald M. Maggiora,*[3] Lester L. Shipman,[4] and Ralph E. Christoffersen*[1]

Contribution from the Departments of Chemistry and Biochemistry, University of Kansas, Lawrence, Kansas 60045, and the Chemistry Division, Argonne National Laboratory, Argonne, Illinois 60439. *Received December 30, 1976*

Abstract: Ab initio SCF-MO calculations on magnesium porphine, magnesium chlorin, ethyl chlorophyllide *a*, and the ethyl chlorophyllide *a*·H_2O adduct have been carried out using the molecular fragment procedure. Molecular orbital energies and ordering, and the correlation of specific orbitals among the molecules, have been examined in detail. The calculations show the expected approximate separation of the HOMO, HOMO − 1, LUMO, and LUMO + 1 from the remainder of the MO manifold as was also seen for the corresponding free bases, in keeping with the four-orbital model. Isodensity contour plots of occupied and unoccupied molecular orbitals indicate substantial similarities, both to each other and to the corresponding magnesium-free molecules. Ionization potential estimates are consistent with the greater ease of electrochemical oxidation of the magnesium-containing species in comparison to their corresponding free bases. Charge and bond orders are examined. In magnesium porphine and magnesium chlorin, the bonding picture that emerges is one of localized π bonds in the periphery of the pyrrolic rings, with a path of conjugation which includes the methine carbons and the "inner parts" of the pyrrolic rings. In ethyl chlorophyllide *a*, the π bonds of the carbonyl group of the isocyclic ring and the vinyl group are mostly localized, but connected to the rest of the π system with nonnegligible bond orders, making the path of conjugation in the macrocycle somewhat less clear. The π-type electron populations on the methine carbons are also consistent with observed deuterium exchange data, C_δ being the most susceptible methine position, in ethyl chlorophyllide *a*. Except for the approximate symmetrization of the electron populations of the pyrrolic nitrogens, a considerable number of similarities exist between the magnesium and corresponding free base species. Examination of the ethyl chlorophyllide *a*·H_2O adduct indicates that very little change in the electronic structure of ethyl chlorophyllide *a* occurs upon H_2O addition, except in the region of the magnesium nucleus. Finally, molecular electrostatic isopotential maps have been constructed and an analysis of the long-range electrostatic field and its relationship to intermolecular interactions is discussed.

In the companion paper preceding in this issue (part 1), various features of the electronic structure of free base porphine, chlorin, and ethyl pheophorbide *a* were described, and comparisons among the molecules were made. In the present paper, analogous studies on the corresponding magnesium-containing molecules will be described, including magnesium porphine, magnesium chlorin, ethyl chlorophyllide *a*, and the ethyl chlorophyllide *a*·H_2O adduct. The discussion will focus on the similarities and differences among the various magnesium-containing species, and will consider the changes that are brought about as a result of magnesium addition, through comparisons to the corresponding magnesium-free species.

Methodology

The various magnesium-containing molecules included in this study are depicted in Figure 1. The theoretical and computational techniques and units[5] used in this study are the same as those described in the previous study of magnesium-free species, and the notation will be the same as that of the preceding companion paper.

For description of the magnesium moiety, two different molecular fragments (MgH_4^{2-} and MgH_6) were developed, and thus the effect of basis set choice can be assessed. The two fragments describe magnesium in an environment of C_{4v} and O_h symmetry, and the optimized parameters are given in Table 1.

For nuclear coordinates, the studies of Zerner and Gouterman[6] were used to give the porphyrin ring structure for magnesium porphine, and the coordinates of the magnesium nucleus in each of the three molecules were taken from the ethyl chlorophyllide *a* crystal structure. The magnesium chlorin coordinates were taken as appropriately idealized modifications of the magnesium porphine strucuture.[7] For ethyl chlorophyllide *a*, the x-ray studies of Strouse[8,9] were used, with minor idealization. In this structure, the four nitrogen nuclei are approximately coplanar and the magnesium nucleus is located at +0.40 Å above the plane of the nitrogen nuclei. For the ethyl chlorophyllide *a*·H_2O adduct, the Strouse studies[8,9] were also used. The atomic Cartesian coordinates for the molecules used in this study are available on request.

It is also perhaps of interest to note that, as an example of the computing resources needed for these studies, the SCF studies on ethyl chlorophyllide *a* (340 electrons, with 277 FSGO contracted to 241 basis functions for the SCF calculation) required a total of approximately 3 h on an IBM 370/195 computer to complete the entire SCF calculation. This includes ~1 for the integral evaluation and ~2 h for SCF iterations.

Results and Discussion

Molecular Orbital Energies. In Figure 2, the energies for several high-lying occupied and low-lying unoccupied molecular orbitals (MO) of magnesium porphine, magnesium chlorin, and ethyl chlorophyllide *a* are given, along with the MO correlations among these molecules. The MgH_4^{2-} fragment was used in each of these studies. In addition, quantitative measures were used to establish these correlations, and they are listed in Table II.

Considering first the MOs of the four-orbital model, it is seen that the approximate isolation of the four orbitals is maintained, and introduction of magnesium has little effect on the relative behavior of MO energies of the four-orbital model. In particular, the trends seen in going from magnesium porphine to magnesium chlorin to ethyl chlorophyllide *a* are

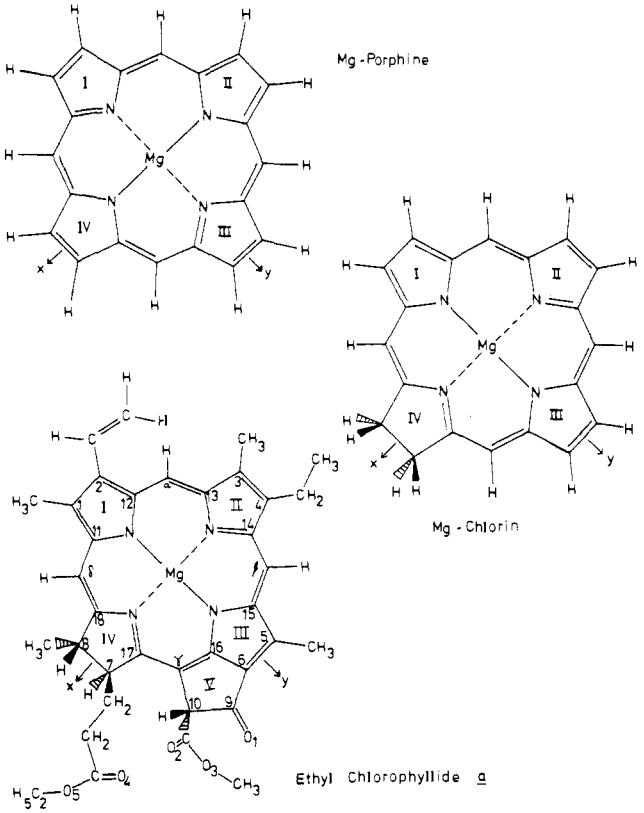

Figure 1. Magnesium-containing molecules included in this study. Only one of several possible resonance structures is shown for convenience.

Table I. Optimized FSGO Parameters for Magnesium Fragment Descriptions

FSGO Type	R,[b] Bohrs	ρ, Bohrs
A. The MgH_4^{2-} Fragment[a]		
Mg-1s	−0.000 012 0	0.156 791 9
Mg-2s	+0.001 976 1	0.786 007 8
Mg-2p_x, 2p_y, 2p_z	±0.1	0.629 549 3
MgH bonds	3.135 394 5	2.303 897 5
B. The MgH_6 Fragment[c]		
Mg-1s	0.0	0.156 774 71
Mg-2s	0.0	0.785 453 35
Mg-2p_x, 2p_y, 2p_y	±0.188 973 0	0.625 307 72
MgH bonds	3.080 712 0	2.143 442 30

[a] The MgH_4^{2-} fragment was chosen to have C_{4v} symmetry, with the four hydrogen nuclei in a plane 0.4012 Å below the magnesium nucleus. The geometric parameters used for the nuclei were R_{MgH} = 1.731 Å, ∠HMgH = 86.9°. Also, the angle from the C_4 axis to any nucleus was taken as 103.4°. [b] Positive values indicate a position along the C_4 axis, toward the plane containing the hydrogen nuclei. The magnesium nucleus was chosen as the origin of the coordinate system. [c] The MgH_6 fragment was chosen to have O_h symmetry, with an optimized distance of 1.795 Å.

quite similar to the trends observed for the corresponding magnesium-free species. More quantitatively, there are a few differences, however. For example, the HOMO in ethyl chlorophyllide *a* appears at higher energy than in ethyl pheophorbide *a*, thus giving rise to the expectation that ethyl chlorophyllide *a* will have a lower first ionization potential than ethyl pheophorbide *a*, based upon a Koopman's theorem[11] estimate.

More generally, the introduction of magnesium is seen to have primarily a "field" effect, since direct contributions to MOs by magnesium orbitals occur only for relatively low-lying MOs. Nevertheless, some interesting effects are seen. For

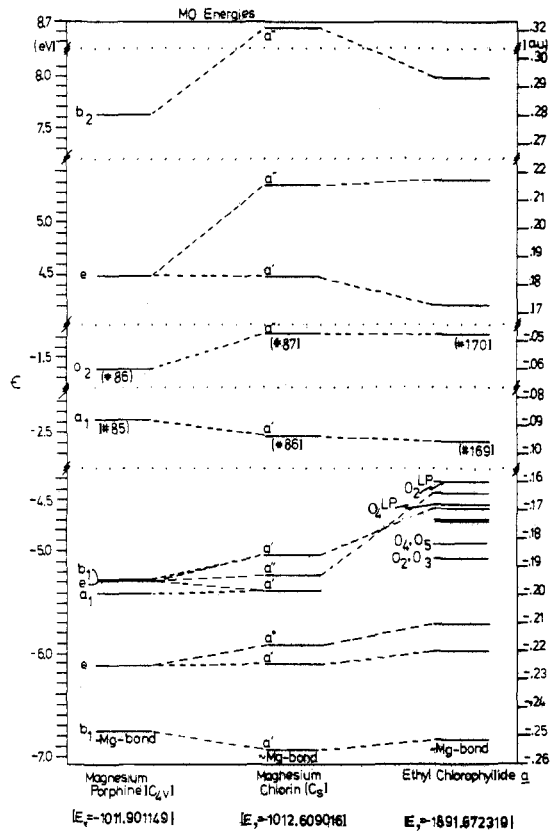

Figure 2. Molecular orbital energies of several high-lying occupied and low-lying unoccupied orbitals of three magnesium-containing species related to chlorophyll. Note that, owing to the slight out-of-plane skewing brought about by reduction of the C_7–C_8 double bond in magnesium porphine, the C_s symmetry in magnesium chlorin is only approximate. Except where indicated, all molecular orbitals are π-type orbitals. All MOs with negative energy are filled, and all those with positive energy are unfilled. MO correlations are indicated by dashed lines. All correlations with $\tau_{ij}^2 \geq 0.25$ (see eq 5 of the preceding companion paper) are included in the figure. Orbitals labeled [O] are mixtures of π and lone pair basis functions located on the oxygens.

example, below the four-orbital MOs, where MO energies are generally closer together, a different "band structure" is seen in the magnesium-containing species compared to their magnesium-free counterparts. In particular, while significant energy changes were observed when the MOs of the magnesium-free species were considered, the corresponding correlations in the magnesium-containing species were substantially less drastic. In other words, the "band structure" is retained to a somewhat greater extent in the magnesium-containing species.

In addition, the "inductive" effect of magnesium affects the MOs in different ways. For example, the HOMO in each of the three molecules is destabilized by approximately 0.2–0.3 eV upon introduction of magnesium, while the corresponding effect on the HOMO − 1 is a stabilization upon magnesium introduction, relative to ethyl pheophorbide *a*.

There are other detailed differences that also are of interest in this regard. For example, changes are seen in the relative ordering of the $C_9{=}O_1$ and O_2 (lone pair) MOs in ethyl chlorophyllide *a* in comparison to those in ethyl pheophorbide *a*. These changes may have an effect on electronic spectral features. Also, the b_2 MO (80) in free base chlorin is seen to be absent in magnesium chlorin, where a "band" of a′ and a″ MOs appears instead. This also affects the correlation of MOs to ethyl chlorophyllide *a*, where MO 85 in magnesium chlorin correlates in a different manner energetically than MO 80 in free base chlorin.

Table II. Calculated Correlations between Molecular Orbitals of Magnesium-Containing Molecules[a,b]

Magnesium porphine MO i	Magnesium chlorin MO j	τ_{ij}^2	Magnesium chlorin MO i	Ethyl chlorophyllide a MO j	τ_{ij}^2
89	90	0.670	90	173	0.523
	89*	0.150		174	0.235
	57	0.048		175	0.102
				176	0.052
88*	88*	0.971	89*	172*	0.925
87*	89*	0.748	88*	171*	0.899
	87*	0.057			
	57	0.045			
86*	87*	0.899	87*	170*	0.930
85*	86*	0.969	86*	169*	0.947
84	83	0.366	85	165	0.735
	85	0.363		167	0.112
83	85	0.531	84	167	0.308
	74	0.071		164	0.203
	66	0.058		160	0.146
	35	0.047		168	0.055
	81	0.041		163	0.051
				159	0.050
				152	0.042
82	84	0.953	83	164	0.210
	82	0.041		163	0.199
				167	0.194
				168	0.074
				157	0.065
				165	0.063
				152	0.049
81	83	0.608	82	160	0.690
	85	0.104			
	74	0.045			
80	82	0.890	81	159	0.828
				160	0.046
79	81	0.893	80	158	0.843
78	80	0.910			
	77	0.072			

[a] See eq 5 and ref 16 of the preceding companion paper for the method of calculation of τ_{ij}^2. The MgH_4^{2-} fragment description was used in each of the above calculations. [b] An asterisk indicates a four-orbital model MO.

The MO energy data found here also suggest that rationalization of the ^{13}C and ^{15}N NMR chemical shifts of chlorophyll a and methyl pheophorbide a given earlier[12] may need reinterpretation. For example, the delocalized nature of the MO structure indicates that consideration of the effect of magnesium only on nitrogen atom energy levels is not sufficient. Furthermore, while introduction of magnesium does raise the HOMO − 1 energy (the HOMO − 1 has a substantial density on the nitrogen nuclei) in magnesium porphine, there is a much greater effect on the HOMO, which has no contribution from the nitrogens. Also, in ethyl chlorophyllide a, there is a stabilization, not destabilization, of the HOMO − 1 compared to ethyl pheophorbide a, regardless of which fragment description is used for ethyl chlorophyllide a. Furthermore, there is no evidence of a high-lying occupied σ MO having nitrogen lone pair character, which was used in the earlier NMR data rationalization.[12] An alternative rationalization of the ^{15}N data in terms of π-type electron populations is given in the following section.

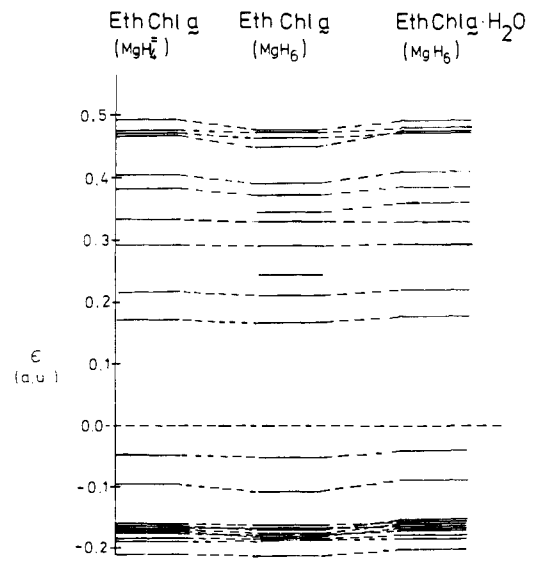

Figure 3. Molecular orbital energies for several high-lying occupied and low-lying unoccupied orbitals for ethyl chlorophyllide a. Three cases are presented, i.e., ethyl chlorophyllide a using an MgH_4^{2-} fragment description, ethyl chlorophyllide a using an MgH_6 fragment description, and ethyl chlorophyllide a·H_2O using an MgH_6 fragment description.

To allow comparison of calculated MO energies to ionization potentials, the data in Table III have been obtained in the manner described for the corresponding magnesium-free species in the companion paper. The approximate degeneracy of the first ionization potential of magnesium chlorin and ethyl chlorophyllide a is seen, analogous to the free-base species. These small shifts to lower ionization potentials upon magnesium introduction are consistent with the relatively constant differences in first and second oxidation potentials reported experimentally.[13] It is also of interest to note that the estimated first ionization potential of ethyl chlorophyllide a is in excellent agreement with an experimentally estimated value[14] of 6.1 eV. Also, lowering of the first ionization potential by ~0.2–0.3 eV

Table III. Ionization Potential Estimates[a] for Magnesium Porphine, Magnesium Chlorin, and Ethyl Chlorophyllide *a*

Molecule	Molecular orbital No.	Molecular orbital Type[b]	Ionization potential estimate, eV[c]
Magnesium porphine	86	$a_2(\pi)$	6.4
	85	$a_1(\pi)$	7.1
	84	$b_1(\pi)$	9.6_7
	83,82	$e(\pi)$	9.6_8
	81	$a_1(\pi)$	9.8
	80,79	$e(\pi)$	10.4
Magnesium chlorin	87	$a''(\pi)$	6.1
	86	$a'(\pi)$	7.2
	85	$a'(\pi)$	9.5
	84	$a''(\pi)$	9.6
	83	$a'(\pi)$	9.8
	82	$a''(\pi)$	10.2
Ethyl chlorophyllide *a*	170	π	6.1 (6.2)
	169	π	7.3 (7.6)
	168	n[d]	8.8 (8.9)
	167	π	$8.9\ (9.0_4)$
	166	n[e]	$9.0\ (9.0_6)$
	165	π	$9.1\ (9.2_0)$
	164	π	$9.1_5\ (9.2_1)$
	163	π	$9.1_7\ (9.3_7)$
	162	$n + \pi$[f]	$9.4\ (9.3_8)$
	161	$n + \pi$[g]	9.5 (9.5)
	160	π	10.1 (10.1)

[a] Ionization potential estimates given in the table are based upon the use of eq 6 of the preceding companion paper, the data from Figure 3, and Koopman's theorem (see ref 11). [b] Note that the MO type designation is only approximate since magnesium lies slightly out of the plane of the macrocycle. Additional nonplanarities are also present in magnesium chlorin and ethyl chlorophyllide *a*. [c] Ionization potential estimates for ethyl chlorophyllide *a* were obtained with the MgH_4^{2-} fragment. Values obtained with the MgH_6 fragment are given in parentheses. [d] Lone pair (O_2). [e] Lone pair (O_4). [f] Lone pair (O_3, O_1) + π (C=O_2). [g] Lone pair (O_5) + π (C=O_4).

in ethyl chlorophyllide *a* compared to ethyl pheophorbide *a* is consistent with the experimental observation[15] that electrochemical oxidation of chlorophyll to the π cation radical is more difficult by approximately 0.3 eV for the free base than for the metal complex.

The effect of the choice of magnesium fragment description can also be assessed from these data. In Figure 3, the MO energies for ethyl chlorophyllide *a* are given for several high-lying occupied and low-lying unoccupied MOs, using both fragment descriptions. Also given are the corresponding MO energies for the ethyl chlorophyllide *a*·H_2O adduct. As the figure illustrates, MO ordering changes do not occur in general, except in the low energy "band-type" regions. Instead, the only significant change is the appearance of a new virtual MO (LUMO + 2) which occurs when the MgH_6 fragment is used. This virtual MO, which is localized above the magnesium nucleus in ethyl chlorophyllide *a*, becomes the acceptor MO for the oxygen lone pairs of H_2O in the ethyl chlorophyllide *a*·H_2O adduct. In the latter case, the former LUMO + 2 becomes filled, and appears in the manifold of MO energies below those depicted in Figure 3. Other than that, very few changes are seen, either in the MgH_4^{2-} or MgH_6 fragment descriptions, or in the ethyl chlorophyllide *a*·H_2O adduct. This independence of the higher occupied and lower unoccupied MOs to H_2O addition is consistent with the observation[16] that the $S_1(\pi,\pi^*) \leftarrow S_0$ electronic transition in monomeric chlorophyll *a* is insensitive to the ligand coordinated to magnesium.

Molecular Orbital Shapes. For comparisons among the various magnesium-containing species, as well as their magnesium-free counterparts, electron density contour maps of the top two occupied (HOMO, HOMO − 1) and hole density

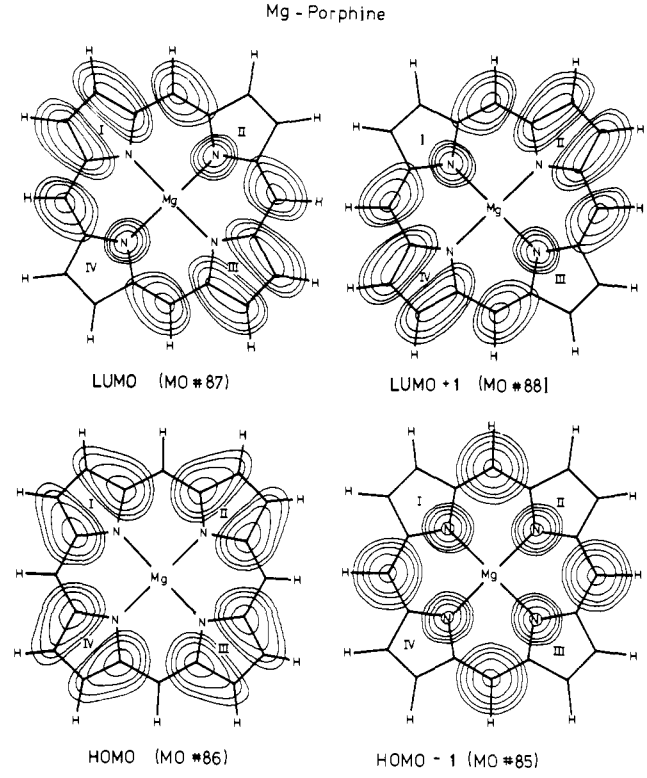

Figure 4. Electron density contour maps for the LUMO, LUMO + 1, HOMO, and HOMO − 1 of magnesium porphine. Contours are at levels of 10, 20, 40, 80, and 160 millielectrons/(Bohr)^3, and are constructed for a plane 1.0 Bohr above the macrocycle plane.

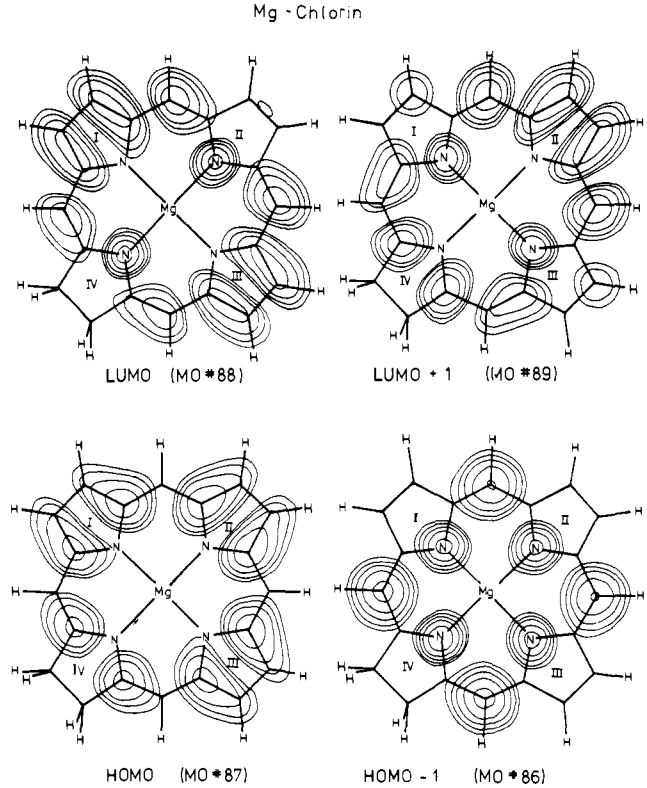

Figure 5. Electron density contour maps for the LUMO, LUMO + 1, HOMO, and HOMO − 1 of magnesium chlorin. Contours are at levels of 10, 20, 40, 80, and 160 millielectrons/(Bohr)^3, and are constructed for a plane 1.0 Bohr above the macrocycle plane.

contour maps of the bottom two unoccupied (LUMO, LUMO + 1) orbitals, which together constitute the MOs of the four-orbital model, are given in Figures 4–7.

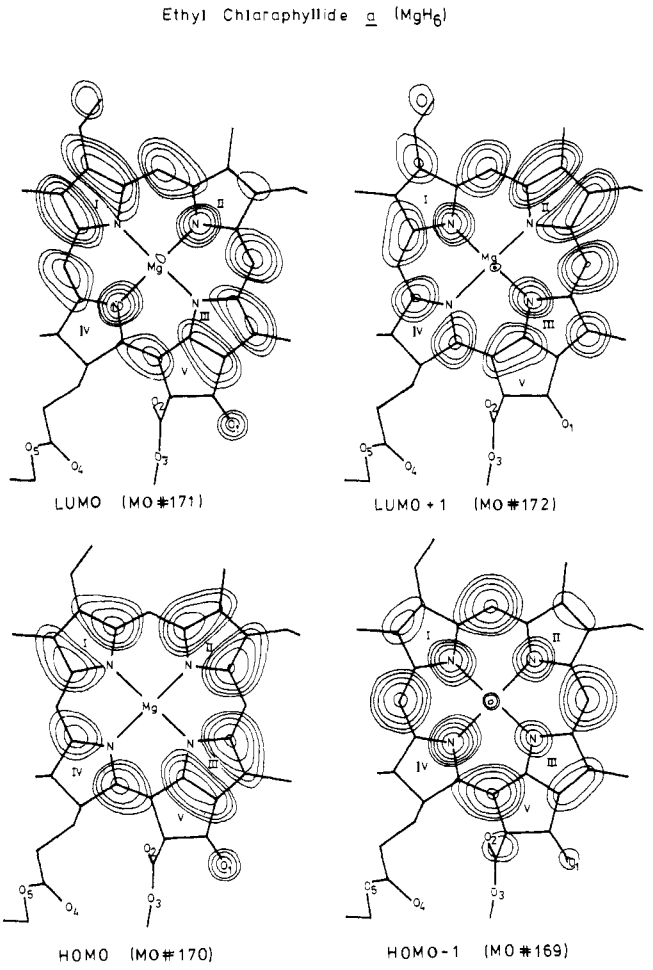

Figure 6. Electron density contour maps for the LUMO, LUMO + 1, HOMO, and HOMO − 1 of ethyl chlorophyllide *a*. Contours are at levels of 10, 20, 40, 80, and 160 millielectrons/(Bohr)^3, and are constructed for a plane 1.0 Bohr above a plane containing approximately all four nitrogen nuclei, using the MgH_6 fragment description.

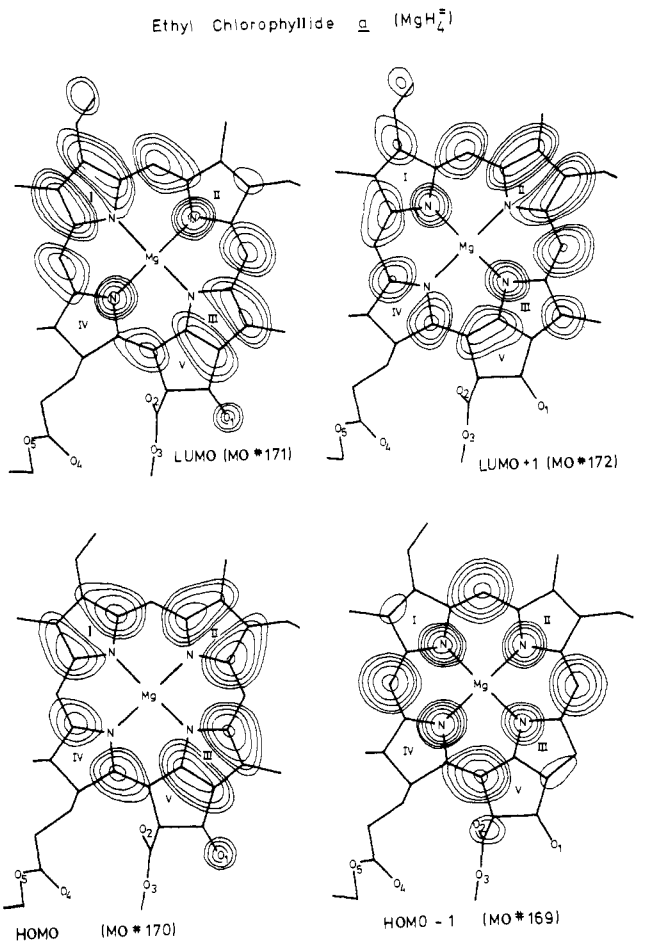

Figure 7. Electron density contour maps for the LUMO, LUMO + 1, HOMO, and HOMO − 1 of ethyl chlorophyllide *a*. Contours are at levels of 10, 20, 40, 80, and 160 millielectrons/(Bohr)^3, and are constructed for a a plane 1.0 Bohr above a plane containing approximately all four nitrogen nuclei, using the MgH_4^{2-} fragment description.

Considering first the HOMO of each of the molecules, it is seen that the introduction of magnesium has virtually no effect on the shape of the HOMO in magnesium porphine compared to free base porphine. Similar comments also apply to the HOMO in magnesium chlorin and in free base chlorin. For ethyl chlorophyllide *a*, it is seen that the HOMO description is virtually the same for both fragment descriptions, and this description is the same as the HOMO in ethyl pheophorbide *a*. Therefore, the introduction of magnesium can be considered to have essentially no effect on the shape of the HOMO in each of the three magnesium-containing molecules compared to their corresponding magnesium-free analogues, and trends in the HOMO shape noted for the magnesium-free species apply equally well in the magnesium-containing analogues. Also, the HOMO in each species is clearly a π-type MO, indicating that formation of the cation would produce a π cation radical,[17] as opposed to ionization of the metal. This is consistent with the observation[18] that the ESR signal from oxidized monomeric chlorophyll has a *g* value quite near that for a free electron, and further indicates that the unpaired electron is quite delocalized.

Since a π cation is expected, and since the HOMO and HOMO − 1 in ethyl chlorophyllide *a* are relatively well separated energetically, it is expected that the relative lack of π population on the methine carbons and nitrogen nuclei will result in an absence of hyperfine interactions involving either kind of nuclei. This is also consistent with available experimental evidence.[19,20]

For both magnesium porphine and magnesium chlorin, the HOMO − 1 are very similar, both to each other and to their corresponding magnesium-free analogues. The only minor differences occur in the lack of density in the C_1–C_2 and C_5–C_6 regions of rings I and III, respectively, in the magnesium-containing analogues. For ethyl chlorophyllide *a*, several differences are discernible. For example, both magnesium fragment descriptions of ethyl chlorophyllide *a* indicate density in the C_{10a}–O_2 region, while none is present in that region in ethyl pheophorbide *a*.

There are also some differences arising from the magnesium fragment description that are seen in this MO in ethyl chlorophyllide *a*. For example, the MgH_6 fragment description indicates density in the magnesium region and the C_9–O_1 region that is not present in the MgH_4^{2-} description. Also, minor changes in the C_1–C_2, C_3–C_4, and C_5C_6 regions are seen. Speaking approximately, the HOMO − 1 shape obtained from the MgH_4^{2-} fragment more closely resembles the HOMO − 1 in magnesium porphine and magnesium chlorin, while the shape obtained from the MgH_6 fragment is more extended throughout the macrocycle and peripheral substituents.

Proceeding to the LUMO, it is seen that the LUMO in magnesium porphine corresponds to the LUMO + 1 in free base porphine, with both having very similar shapes. Other than that, the LUMO in magnesium-containing analogues, and trends noted for the magnesium-free species, also apply for the magnesium-containing analogues. In addition, both the MgH_4^{2-} and MgH_6 fragments in ethyl chlorophyllide *a* are seen to produce essentially identical MO shapes. It is of interest

Table IV. Electron Populations and Bond Orders for Magnesium Porphine and Magnesium Chlorin[a,b]

Magnesium porphine	Magnesium chlorin	
	A. σ Orbitals	
	Bond Populations[c,d]	
N_2–Mg: 2.100 (0.920)	N_2–Mg: 2.105 (0.919)	
	N_3–Mg: 2.092 (0.919)	
	N_4–Mg: 2.114 (0.918)	
	B. π Orbitals	
	Atom Populations	
N_2: 1.326	N_2: 1.296	
C_{14}: 0.995	C_{14}: 1.043	
C_4: 1.033	C_4: 1.048	
C_β: 1.112	C_β: 1.071	
	C_{15}: 1.029	
	C_5: 1.008	
	N_3: 1.343	
	C_6: 1.060	
	C_{16}: 0.961	
	C_γ: 1.208	
	C_{17}: 0.992	
	N_4: 1.244	
	Bond Orders[e]	
N_2–C_4: −0.211	N_2–C_4: −0.221	C_{15}–C_5: 0.402
N_2–C_{14}: 0.582	N_2–C_{14}: 0.589	C_{15}–N_3: 0.527
C_4–C_{14}: 0.408	C_4–C_{14}: 0.441	C_5–C_6: 0.833
C_3–C_4: 0.833	C_3–C_4: 0.811	C_5–N_3: −0.236
C_{14}–C_β: 0.589	C_{14}–C_β: 0.552	C_{16}–N_3: 0.624
	C_β–C_{15}: 0.644	C_6–C_{16}: 0.413
	C_β–C_{16}: −0.225	C_{16}–C_γ: 0.530
		C_γ–C_{17}: 0.661
		C_{17}–N_4: 0.600

[a] See ref 22. [b] The MgH_4^{2-} fragment was used. [c] Bond orders between adjacent FSGO in the bonding region are given in parentheses. [d] Populations for FSGO in the bonding regions are given as the sum of the population of each of the two FSGO in the bonding region. [e] All π-type bond orders $>|0.2|$ are given.

to note that the contributions from the vinyl group at C_2 and the C_9=O_1 keto group in ethyl chlorophyllide *a* remain present and essentially unchanged from ethyl pheophorbide *a*.

For the LUMO + 1, changes in ring IV and at C_1 and C_5 in magnesium chlorin compared to magnesium porphine are seen, similar to those observed in the corresponding magnesium-free species. From magnesium chlorin to ethyl chlorophyllide *a*, very few changes are observed, except for the addition of a small amount of hole density in the vinyl group region at C_2. Also, only very minor differences in the fragment descriptions are seen.

Summarizing, for the case of the four-orbital MO, very little effect of magnesium addition is seen on their shapes. This description indicates substantial vinyl and ring V keto group contributions[21] to the π system of ethyl chlorophyllide *a*, and a minor contribution from the C_{10a}=O_2 keto group to the π system. The other ester moiety (at C_{7c}) is apparently localized, and does not contribute to the macrocycle π system.

Electron Populations and Bond Orders.[22] In order to discuss the total charge distribution in each of the magnesium-containing species and compare these to the corresponding magnesium-free species, electron populations and bond orders for the various molecules studied here are presented in Tables IV–VII.

Considering the σ-type populations first, we note that the N–H and N(LP) populations in free base porphine become symmetrized in magnesium porphine as expected. In magnesium chlorin, a similar effect is seen, except that the asymmetry introduced by reduction of the C_7–C_8 bond is reflected in a slight asymmetry in the N–Mg populations, with the N_2–Mg and N_4–Mg populations being slightly higher than the N_3–Mg (and N_1–Mg) populations. In ethyl chlorophyllide *a*, the slight asymmetry in N–Mg populations is present again, although the magnitude of the bond populations depends somewhat upon the particular fragment description employed. The other effect associated with fragment choice is the introduction of small populations in the fragment Mg^u and Mg^d basis orbitals in the MgH_6 description (see Table VI). Thus, one of the first general observations of interest concerning the effect of magnesium introduction is the appearance of σ-bonding population in the N–Mg region.

The various oxygen σ-type populations are seen to be essentially invariant to both magnesium introduction and magnesium fragment description, with the σ-type populations of the carbonyl oxygens higher than those of the ether oxygens.

In the case of C–C and C–N σ-type bond populations, virtually no change is seen between free base and magnesium porphine. Similarly, only very small changes are seen in going from free base to magnesium chlorin or from ethyl pheophorbide *a* to ethyl chlorophyllide *a* and, therefore, these populations have not been given in the tables.

Turning next to the π-type orbital populations, we note first the expected symmetrization of π density on the nitrogen nuclei when magnesium is introduced into free base porphine.[12,23] In addition, this "averaging" process implies that no substantial π density is transferred from the ring system to the magnesium nucleus upon its introduction. Also, the carbon atom π populations are seen to show much smaller changes than those for nitrogen upon magnesium introduction into free base porphine.

Comparing magnesium chlorin to free base chlorin, it is seen that the N_1 (and N_3) π populations increase upon magnesium introduction, while the N_2 (and N_4) populations decrease. This is similar to the effect in free base and magnesium porphine, except that the basic asymmetry in the π population distribution brought about by the C_7–C_8 bond reduction is reflected in both free base and magnesium chlorin. In addition, the C_β (and C_α) and C_{15} (and C_{12}) π populations are decreased upon magnesium introduction, and a relative increase in C_γ (vs. C_β) population is also seen in comparing magnesium chlorin to magnesium porphine. The C_{14} π population (and others related by symmetry) in magnesium porphine and the C_{16} and C_{17} π populations in magnesium chlorin are relatively electron deficient. While this effect is also seen in free base chlorin, it is absent in free base porphine, where all carbon atom π populations are >1.0.

Comparing ethyl chlorophyllide *a* to ethyl pheophorbide *a*, a variety of changes are apparent in the π-type populations. For example, similar to those in free base and magnesium chlorin, increases in the N_2 and N_4 populations are seen upon magnesium introduction, along with reductions in the N_1 and N_3 π populations. In addition, a slight increase in total π population of the four nitrogens is observed in ethyl chlorophyllide *a* (5.273) relative to ethyl pheophorbide *a* (5.259). This is in contrast to the case of chlorin, where a slight decrease in total π population of the four nitrogens is observed in magnesium chlorin (5.226) relative to its free base (5.244).

In the carbon atom π-type populations, decreases at C_{15}, C_{10a}, C_{18}, C_{11}, C_1, C_{12}, and C_{13} in ethyl chlorophyllide *a* (MgH_4^{2-} description) are observed relative to ethyl pheophorbide *a*, while increases are seen at C_{14} and C_2. In addition, the π populations of the methine carbons appear in the order $C_\delta > C_\alpha > C_\beta$, which is the same as that observed in ethyl pheophorbide *a*. Furthermore, the methine carbon populations in ethyl chlorophyllide *a* are greater than the corresponding populations in ethyl pheophorbide *a*, implying a faster proton/deuterium exchange rate in ethyl chlorophyllide *a*. These observations are consistent with observed rates of deuterium exchange at these positions,[23,24] to the extent that the

Table V. Electron Populations and Bond Orders for Ethyl Chlorophyllide *a* (MgH_4^{2-} Fragment)[a]

A. σ Orbitals

Bond Populations[b,c]

N_1–Mg: 2.088 (0.923)	N_4–Mg: 2.114 (0.919)	O_2: 1.986	O_{32}: 1.860	O_{51}: 1.857
N_2–Mg: 2.098 (0.920)	O_1: 1.994	O_2^{PLP}: 1.924	O_4: 1.991	O_{52}: 1.870
N_3–Mg: 2.088 (0.918)	O_1^{PLP}: 1.961	O_{31}: 1.874	O_4^{PLP}: 1.932	

B. π Orbitals

Atom Populations

N_2: 1.304	C_5: 1.039	O_1: 1.007	N_4: 1.266	C_{11}: 0.939	C_{2a}: 0.970
C_{14}: 1.062	N_3: 1.329	C_{10a}: 1.125	C_{18}: 0.962	C_1: 1.048	C_{2b}: 1.056
C_4: 1.044	C_6: 1.087	O_2: 1.170	C_{7c}: 1.145	C_2: 1.013	C_α: 1.126
C_β: 1.044	C_{16}: 0.984	C_γ: 1.160	O_4: 1.143	C_{12}: 0.992	C_{13}: 1.009
C_{15}: 1.070	C_9: 1.071	C_{17}: 1.030	C_δ: 1.247	N_1: 1.374	C_3: 1.083

Bond Orders[d]

Macrocycle Only

N_2–C_4: −0.243	C_6–C_{16}: 0.438	N_1–C_2: −0.220
N_2–C_{14}: 0.529	N_3–C_6: −0.200	C_1–C_2: 0.806
C_4–C_{14}: 0.408	C_{16}–C_γ: 0.456	C_2–C_{12}: 0.343
C_{13}–C_β: −0.216	C_γ–C_{17}: 0.724	C_α–C_{11}: −0.224
C_3–C_4: 0.791	C_{17}–N_4: 0.519	C_α–C_{12}: 0.687
C_{14}–C_β: 0.624	N_4–C_{18}: 0.659	N_1–C_{12}: 0.519
C_β–C_{15}: 0.594	N_4–C_δ: −0.206	C_{13}–C_α: 0.502
C_{15}–C_5: 0.486	C_δ–C_{18}: 0.609	C_3–C_{13}: 0.420
C_{15}–N_3: 0.490	C_{18}–C_γ: −0.220	N_2–C_{13}: 0.640
C_5–C_6: 0.724	C_δ–C_{11}: 0.569	N_2–C_3: −0.204
C_5–N_3: −0.242	C_1–C_{11}: 0.379	C_9–C_6: 0.300
C_{16}–N_3: 0.667	N_1–C_{11}: 0.607	

Macrocycle-Peripheral Substituent Bond Orders

C_{2a}–C_2: 0.276	C_{2b}–C_1: −0.227	C_{2b}–C_{2a}: 0.951	O_1–O_5: −0.207	O_1–C_9: 0.930

[a] See ref 22. [b] Bond orders between adjacent FSGO in the bonding region are given in parentheses. [c] Populations for FSGO in the bonding region are given as the sum of the two FSGO in the bonding region. [d] Bond orders involving peripheral substituents only have been omitted. All other π-type bond orders $>|0.2|$ are given.

Table VI. Electron Populations and Bond Orders for Ethyl Chlorophyllide *a* (MgH_6 Fragment)[a]

A. σ Orbitals

Bond Populations[b,c]

N_1–Mg: 2.117 (0.880)	O_1: 1.994	O_{31}: 1.874	O_{51}: 1.857	
N_2–Mg: 2.125 (0.884)	O_1^{PLP}: 1.960	O_{32}: 1.860	O_{52}: 1.870	
N_3–Mg: 2.130 (0.864)	O_2: 1.986	O_4: 1.991	Mg^u: 0.245	
N_4–Mg: 2.139 (0.879)	O_2^{PLP}: 1.924	O_4^{PLP}: 1.932	Mg^d: 0.109	

B. π Orbitals

Atom Populations

N_2: 1.244	N_3: 1.255	O_2: 1.167	O_4: 1.143	N_1: 1.300
C_{14}: 1.056	C_6: 1.084	C_γ: 1.144	C_δ: 1.223	C_{2a}: 0.973
C_4: 1.039	C_{16}: 0.965	C_{17}: 1.026	C_{11}: 0.932	C_{2b}: 1.051
C_β: 1.035	C_9: 1.072	N_4: 1.201	C_1: 1.047	C_α: 1.112
C_{15}: 1.065	O_1: 1.005	C_{18}: 0.952	C_2: 1.008	C_{13}: 0.996
C_5: 1.031	C_{10a}: 1.127	C_{7c}: 1.145	C_{12}: 0.987	C_3: 1.080

Bond Orders[d]

Macrocycle Only

N_2–C_4: −0.230	C_6–C_{16}: 0.451	C_2–C_{12}: 0.351
N_2–C_{14}: 0.505	$C_{16}C_\gamma$: 0.470	C_α–C_{11}: −0.214
C_4–C_{14}: 0.416	C_γ–C_{17}: 0.725	C_α–C_{12}: 0.691
C_{13}–C_β: −0.209	C_{17}–N_4: 0.503	N_1–C_{12}: 0.493
C_3–C_4: 0.785	N_4–C_{18}: 0.629	C_{13}–C_α: 0.512
C_{14}–C_β: 0.629	C_δ–C_{18}: 0.619	C_3–C_{13}: 0.429
C_β–C_{15}: 0.597	C_{18}–C_γ: −0.212	N_2–C_{13}: 0.606
C_{15}–C_5: 0.496	C_δ–C_{11}: 0.580	C_9–C_6: 0.299
C_{15}–N_3: 0.461	C_1–C_{11}: 0.387	
C_5–C_6: 0.717	N_1–C_{11}: 0.572	
C_5–N_3: −0.224	N_1–C_2: −0.207	
C_{16}–N_3: 0.621	C_1–C_2: 0.802	

Macrocycle-Peripheral Substituent Bond Orders

C_{2a}–C_2: 0.275	C_{2b}–C_1: −0.224	C_{2b}–C_{2a}: 0.952	O_1–C_5: −0.204	O_1–C_9: 0.930

C. Magnesium-Macrocycle (σ–π Type)

N_1–(Mg–N_1): 0.239	N_2–(Mg–N_2): 0.218	N_3–(Mg–N_3): 0.262	N_4–(Mg–N_4): 0.216

[a] See ref 22. [b] Bond orders between adjacent FSGO in the bonding region are given in parentheses. [c] Populations for FSGO in the bonding region are given as the sum of each of the two FSGO in the bonding region. [d] Bond orders involving peripheral substituents only have been omitted. All other π-type bond orders $>|0.2|$ are given.

Table VII. Electron Populations and Bond Orders Showing Significant Changes from Ethyl Chlorophyllide *a* to Ethyl Chlorophyllide *a*·H_2O[a]

A. Populations[b]	
σ Orbitals[c] (Macrocycle Only)	
N_4-Mg: 2.163 (0.866)	
π Orbitals (Macrocycle Only)	
C_{16}: 0.979	C_{17}: 1.036 C_{18}: 0.967 N_4: 1.182
B. Bond Orders[c,d]	
C_3-C_{13}: 0.418	N_2-C_{13}: 0.618 N_2-(Mg-N_2): 0.207
C_{14}-C_4: 0.406	N_4-C_{18}: 0.641
C. Mg-H_2O Interactions	
Populations	
Mg^d: 0.682	$O_W{}^{LP}$: 1.729
Mg^u: 0.244	O_W-Mg: 1.660
Bond Orders[d,e]	
$O_W{}^{LP}$-Mg^u: 0.581	(Ow-Mg)-$O_W{}^{LP}$: −0.259
(Ow-Mg)-Mg^d: 0.630	

[a] See ref 22. [b] All elements having population changes greater than 0.015 are given. The value found in ethyl chlorophyllide *a*·H_2O is given in this table. The MgH_6 fragment was used in both ethyl chlorophyllide *a* and ethyl chlorophyllide *a*·H_2O. [c] The same convention for reporting σ-bond populations and π-type atom populations and σ- and π-type bond orders that was used in Tables V and VI is used here. [d] All bond orders whose magnitudes are $\geq|0.2|$ and whose changes are greater than 0.010 are given in this table. The value found in ethyl chlorophyllide *a*·H_2O is given in this table. Mg^u and Mg^d refer to single FSGO located above and below the Mg nucleus, respectively. [e] The Ow-Mg orbital is the oxygen lone pair orbital of H_2O that points toward the magnesium nucleus. $O_W{}^{LP}$ refers to an FSGO describing one of the σ-type lone pairs on the oxygen nucleus in H_2O.

pseudo-first-order rate constant for hydrogen exchange in chlorophyll *a* is more than 40 times greater at C_δ than at either C_α or C_β, and more than 40 times greater than at C_α, C_β, or C_δ of methyl pheophorbide *a*. Similar trends are seen in comparing the $MgH_4{}^{2-}$ and MgH_6 fragment descriptions, with slightly lower π populations being observed in the macrocycle calculated using the MgH_6 description, and the additional π population being transferred to the additional magnesium basis orbitals. For example, the π-type populations on N_1, N_2, N_3, and N_4 are somewhat decreased in the MgH_6 fragment description.

Considering the π-bond orders in the various molecules, several changes are worthy of mention. In magnesium porphine, for example, the N_2-C_{14} and C_3-C_4 π-bond orders are decreased, while the C_4-C_{14} π-bond order has increased, relative to free base porphine. This suggests that essentially only one resonance structure is appropriate for the magnesium-containing species, i.e., A, as compared to two resonance structures for the corresponding free base.

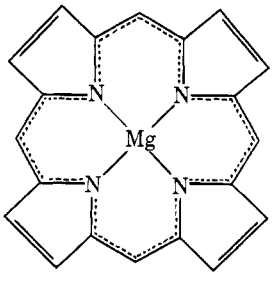

A

Turning to magnesium chlorin, a bonding picture quite similar to that of free base chlorin is found, with a localized π-electron bond found between each pair of exterior carbon atoms of the three nonreduced pyrrole moieties. Thus, as in free base chlorin, the C_7-C_8 bond reduction is again essentially a local effect, in which electron density distribution and bond orders are changes primarily in ring IV only.

For ethyl chlorophyllide *a*, introduction of magnesium causes a variety of rather small changes in π-bond orders compared to ethyl pheophorbide *a*, but the bond picture is quite similar in both molecules. For example, the vinyl and C_9=O_1 keto bonds are again seen to be mostly localized, as well as the C_1-C_2, C_3-C_4, and C_5-C_6 bonds. In addition, the trends toward more localization of π bonds is observed in ethyl chlorophyllide *a* as it was in ethyl pheophorbide *a*, along with the C_{12}-C_α, C_{13}-N_2, C_{14}-C_β, N_3-C_{16}, C_γ-C_{17}, and C_{11}-N_1 bonds showing more localized character compared to magnesium chlorin. Both fragment descriptions give this picture, although the C_{11}-N_1 π bond appears somewhat less localized in the MgH_6 fragment description.

The coordination of H_2O to the magnesium of ethyl chlorophyllide *a* produces several effects. In particular, as seen in Table VII, the N_4-Mg σ bond gains electrons slightly, while the C_{16}, C_{17}, and C_{18} π populations increase slightly. Minor changes are also seen in several π-bond orders. The major change observed is the formation of a Mg-H_2O coordination bond, which is apparent from the substantial increase in Mg^d and Mg^u populations and $O_W{}^{LP}$-Mg^u and $O_W{}^{LP}$-Mg^d bond orders. Thus, as suggested by the MO energy data, the populations and bond orders also suggest that the formation of a water adduct to ethyl chlorophyllide *a* is essentially a localized effect, involving primarily the magnesium and one of the H_2O lone pairs.

The charge distributions and bond orders found here can also be compared to other studies that have been reported. For example, viewing a metalloporphyrin as having a structure such as[13] B does not appear appropriate for several reasons.

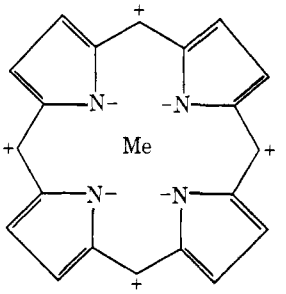

B

First, the π-bond orders indicate localized π bonds on C_1-C_2, C_3-C_4, C_5-C_6, and C_7-C_8 in magnesium porphine, instead of as shown above. Second, since there is essentially no charge transfer from the nitrogen π orbitals to the magnesium in magnesium porphine, its π system and that of free base porphine have essentially the same π populations.[17] Also, the methine populations are actually seen to increase instead of decrease when magnesium is introduced.

Also, in comparing the NMR spectra of methyl pheophorbide *a* with that of chlorophyll *a*, it was concluded[12] that introduction of magnesium indicated the formation of an "anion" in rings I and III. However, computation of the total π density in rings I–III in ethyl pheophorbide *a* and ethyl chlorophyllide *a* indicates total π-populations as follows:

	Ring I	Ring II	Ring III
Ethyl pheophorbide *a*	5.556	5.352	5.681
Ethyl chlorophyllide *a* ($MgH_4{}^{2-}$)	5.366	5.502	5.509
Ethyl chlorophyllide *a* (MgH_6)	5.274	5.415	5.400

In addition, the σ populations also do not indicate substantial asymmetry in the pyrrolic units. Thus, the total π populations indicate an opposite effect upon introduction of magnesium,

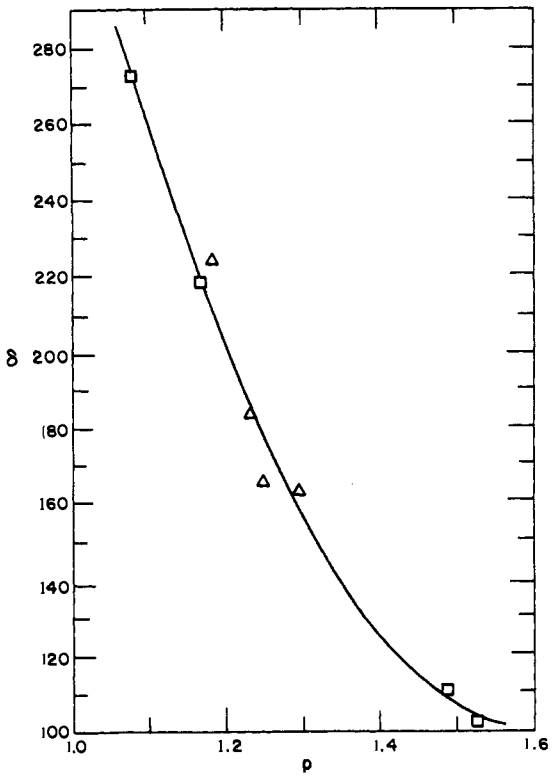

Figure 8. A plot of ^{15}N chemical shifts (in parts per million relative to $^{15}NH_4Cl$) vs calculated nitrogen p-orbital populations. Squares correspond to magnesium-free compounds, and triangles correspond to magnesium-containing compounds.

Table VIII. Comparison of ^{15}N Chemical Shifts[a] and p-Orbital Populations

Nucleus	δ^b ppm	p[c]	δ^d ppm	p[e]
N_1	102.5	1.527	163.6	1.295
N_2	218.5	1.166	183.5	1.231
N_3	110.9	1.488	166.4	1.248
N_4	272.8	1.078	224.0	1.182

[a] ^{15}N chemical shifts are given in parts per million relative to $^{15}NH_4Cl$. [b] ^{15}N chemical shifts in methyl pheophorbide *a*. [c] p-Orbital populations in ethyl pheophorbide *a*. [d] ^{15}N chemical shifts in chlorophyll *a*. [e] p-Orbital populations in ethyl chlorophyllide *a*.

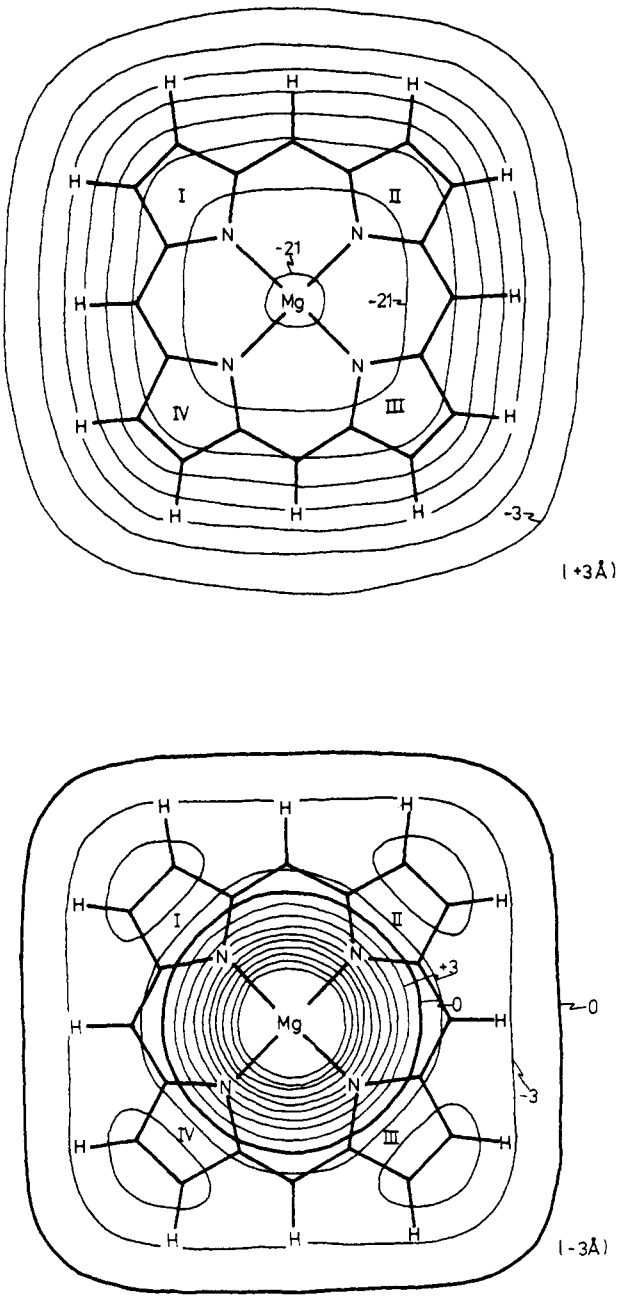

Figure 9. Electrostatic isopotential maps for magnesium porphine, constructed in planes ±3 Å from the macrocycle plane. Contour levels are given in kcal/mol and are in increments of 3 kcal/mol.

i.e., rings I and III have fewer π electrons in ethyl chlorophyllide *a* than in ethyl pheophorbide *a*, and an approximately equal number of π electrons in rings II and IV.

However, other interpretations of the NMR data are consistent with the current studies. In particular, since it is sometimes found that observed chemical shifts at various nuclei can be correlated with the electron density at the corresponding nuclei, a comparison of the π-type populations (p) in ethyl pheophorbide *a* and ethyl chlorophyllide *a* have been compared to observed chemical shifts[12] (δ) in methyl pheophorbide *a* and chlorophyll *a*. In particular, the ^{15}N chemical shifts and corresponding p-orbital populations are given in Table VIII.

A good quadratic correlation has been found between ^{15}N chemical shifts and p-orbital populations. In particular, the following relationship results from a least-squares fit of the ^{15}N chemical shift data to the p-orbital populations:

$$\delta(\text{ppm}) = 1788 - 2127p + 671p^2 \quad (1)$$

The curve calculated from eq 1 is compared pictorially with the data in Figure 8. It is seen that a good correlation of ^{15}N chemical shift data with nitrogen p-orbital populations is observed, with resonance at higher fields corresponding to increasing p-orbital populations. This is consistent with the intuitive rationale for chemical shifts in which greater electron density on an atom causes more shielding from the external magnetic field, and an increased chemical shift. Of course, it should be noted that such comparisons are expected to be only approximate, since only ground-state electron density data from approximate Hartree-Fock calculations have been used for the correlations. An example of a situation where these data are apparently not adequate for correlative purposes is for ^{13}C chemical shift data for these molecules.

Electrostatic Isopotential Maps. While introduction of magnesium generally has somewhat small effects on charge

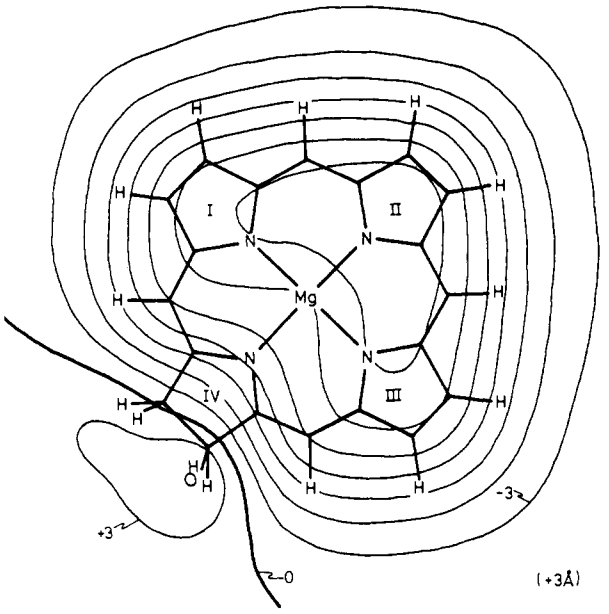

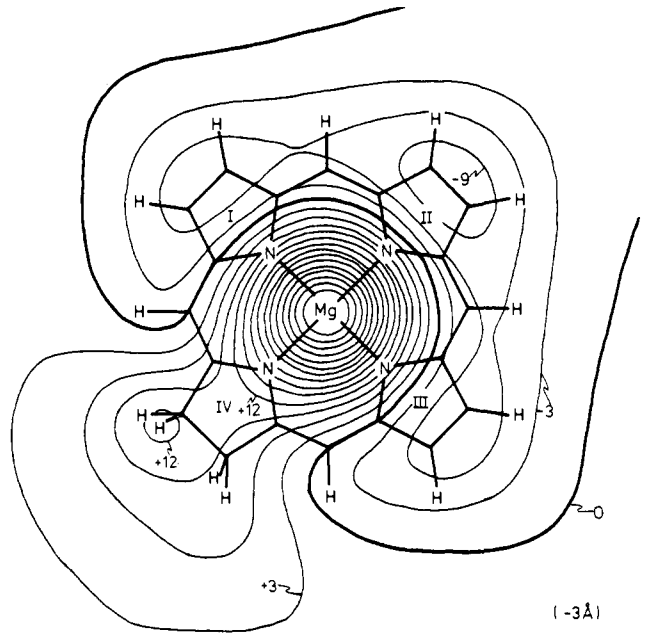

Figure 10. Electrostatic isopotential maps for magnesium chlorin, constructed in planes ±3 Å from the macrocycle plane. Contour levels are given in kcal/mol and are in increments of 3 kcal/mol.

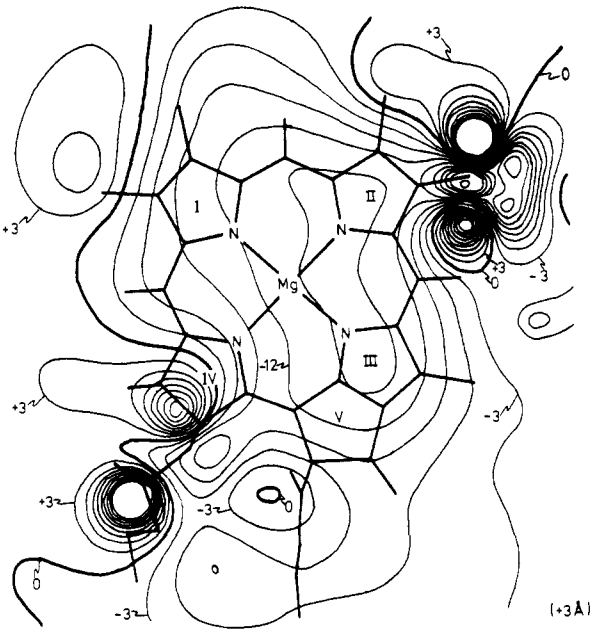

Ethyl Chlorophyllide a (MgH_6)

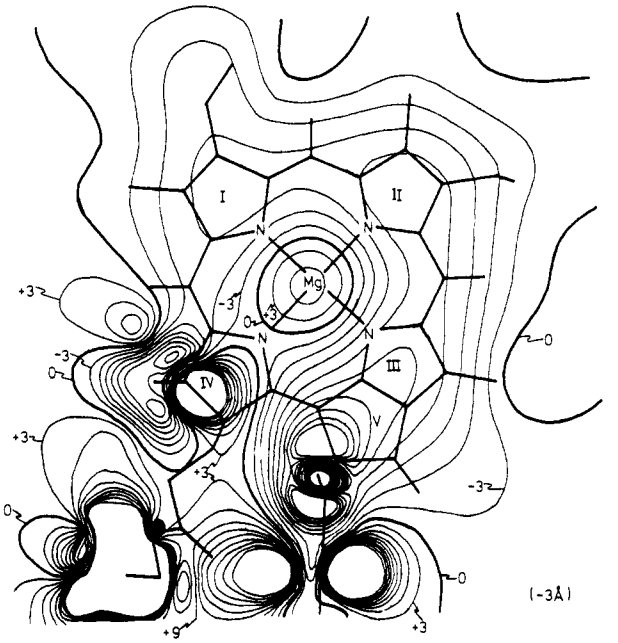

Figure 11. Electrostatic isopotential maps for ethyl chlorophyllide *a*, constructed in planes ±3 Å from a plane containing approximately all four nitrogen nuclei. Contour levels are given in kcal/mol and are in increments of 3 kcal/mol. The electrostatic isopotentials were based on the SCF study using the MgH_6 fragment.

distributions, substantial changes in the potential produced by the charge distributions are seen. So that comparison with the corresponding free bases can be made, molecular isopotential maps for each of the magnesium-containing species are presented in Figures 9–13.

For porphine, the introduction of magnesium is seen to convert a potential which is totally attractive in free base porphine to one which is attractive for approach of a positively charged species in the plane above the macrocycle (where the magnesium nucleus is below the macrocycle), and repulsive for most of the regions in the plane below the macrocycle.

In the case of chlorin, introduction of magnesium again produces a repulsive potential below the macrocycle plane in general, with the region of repulsive potential extended to ring IV as well. Above the plane a generally attractive potential is seen, but ring II is now favored owing to the effect of the repulsive potential created in the C_7–C_8 region of ring IV.

In ethyl chlorophyllide *a*, it is also seen that both the MgH_4^{2-} and MgH_6 fragment descriptions give rise to similar potentials at ±3 Å from the macrocycle plane. In a plane perpendicular to the macrocycle plane (Figure 13), however, several small changes are observed. In particular, in the region below the magnesium nucleus, the MgH_4^{2-} fragment description indicates a repulsive potential throughout, while the

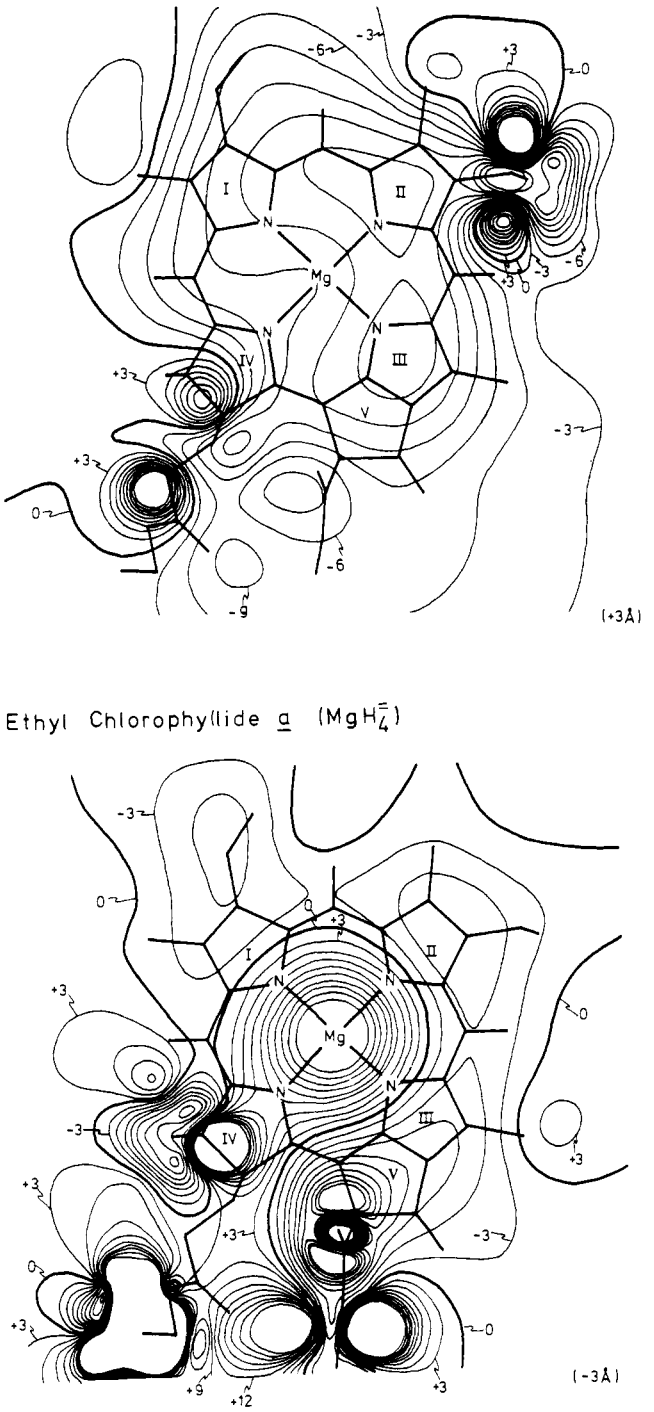

Figure 12. Electrostatic isopotential maps for ethyl chlorophyllide *a*, constructed in planes ±3 Å from a plane containing approximately all four nitrogen nuclei. Contour levels are given in kcal/mol and are in increments of 3 kcal/mol. The electrostatic isopotentials were based on the SCF study using the MgH_4^{2-} fragment.

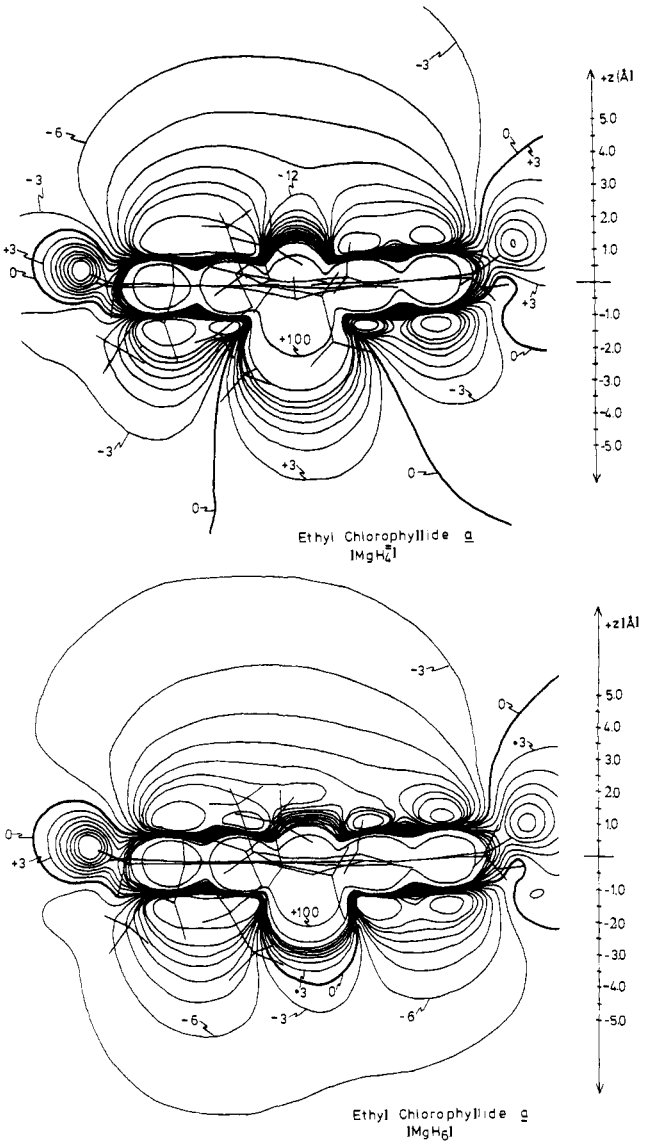

Figure 13. Electrostatic isopotential map for ethyl chlorophyllide *a*, constructed in the *yz* plane as viewed along the positive *x* axis toward the macrocycle (see Figures 1 and 2). Contour levels are given in kcal/mol and are in increments of 3 kcal/mol. The MgH_4^{2-} and MgH_6 fragment descriptions used in the SCF calculations were then used to calculate the isopotential maps for the upper and lower figures, respectively.

MgH_6 description indicates a slightly attractive region beyond approximately −4.0 Å. The overall descriptions are quite similar, however, and indicate attractive regions for ±3 Å in the vicinity of $C_{10a}{=}O_2$ and $C_{7a}{-}O_4$ as well as rings II and III. Below the macrocycle plane (at −3.0 Å) the repulsive region around the magnesium nucleus remains, but weakly attractive potentials are seen also in several areas.

Finally, it is of interest to note that the isopotential maps indicate that an incoming H_2O molecule would coordinate to ethyl chlorophyllide *a* from below (which is the same side as the magnesium atom is located), as suggested earlier.[8,25]

Acknowledgments. This work was supported in part by the Division of Physical Research, U.S. Energy Research and Development Administration. Partial support of some of the computing time required for this study by the University of Kansas is also gratefully acknowledged. We thank Dr. J. J. Katz for many helpful discussions, and Mr. Ross McKinney for help in the initial calculations.

References and Notes

(1) Department of Chemistry, University of Kansas.
(2) Participant in the Argonne Thesis Parts Program.
(3) Department of Biochemistry, University of Kansas.
(4) Argonne National Laboratory.
(5) Unless otherwise stated, all quantities reported are given using Hartree atomic units. See H. Shull and G. G. Hall, *Nature (London)*, **184**, 1559–1560 (1959).
(6) M. Zerner and M. Gouterman, *Theor. Chim. Acta*, **4**, 44–63 (1966).
(7) In order to reduce the strain in ring IV brought about by reduction of the C_7–C_8 bond, a slight out-of-plane twist of the C_7–C_8 bond is required. While this twist further lowers the symmetry of the molecule below C_s, its effect is small and the MOs can still practically, albeit not rigorously, be classified by the irreducible representations of the C_s point group.
(8) C. E. Strouse, *Proc. Natl. Acad. Sci. U.S.A.*, **71**, 325–328 (1973).

(9) H. C. Snow, R. Serlin, and C. E. Strouse, *J. Am. Chem. Soc.*, **97**, 7230–7237 (1975).
(10) Of the two H_2O molecules reported by Strouse, only the one coordinated to magnesium was used in the studies reported here.
(11) T. Koopmans, *Physica*, **1**, 104–113 (1933).
(12) S. G. Boxer, G. L. Closs, and J. J. Katz, *J. Am. Chem. Soc.*, **96**, 7058–7066 (1974).
(13) J. H. Fuhrhop, *Struct. Bonding (Berlin)*, **18**, 1–67 (1974).
(14) Y. Nakato, T. Chiyoda, and H. Tsubomura, *Bull. Chem. Soc. Jpn.*, **47**, 3001–3005 (1974).
(15) J. R. Harbour and G. Tollin, *Photochem. Photobiol.*, **19**, 69–74 (1974).
(16) L. L. Shipman, T. M. Cotton, J. R. Norris, and J. J. Katz, *J. Am. Chem. Soc.*, in press.
(17) This has been observed by G. M. Maggiora, *J. Am. Chem. Soc.*, **95**, 6555–6559 (1973).
(18) J. R. Norris, R. A. Uphaus, H. L. Crespi, and J. J. Katz, *Proc. Natl. Acad. Sci. U.S.A.*, **68**, 625–628 (1971).
(19) D. C. Borg, J. Fajer, R. H. Felton, and D. Dolphin, *Proc. Natl. Acad. Sci. U.S.A.*, **67**, 813–820 (1970).
(20) D. Dolphin and R. H. Felton, *Acc. Chem. Res.*, **7**, 26–32 (1974).
(21) For a description of some of the implications of the charge distribution for chlorophyll *a* dimerization, see L. L. Shipman, T. R. Janson, R. J. Ray, and J. J. Katz, *Proc. Natl. Acad. Sci. U.S.A.*, **72**, 2873–2876 (1975).
(22) See L. L. Shipman and R. E. Christoffersen, *Chem. Phys. Lett.*, **15**, 469–474 (1972), for a detailed discussion of electron population analysis in symmetrically orthogonalized FSGO basis sets.
(23) For an initial report of this effect, see D. Spangler, R. McKinney, R. E. Christoffersen, G. M. Maggiora, and L. L. Shipman, *Chem. Phys. Lett.*, **36**, 427–431 (1975).
(24) R. C. Dougherty, H. H. Strain, and J. J. Katz, *J. Am. Chem. Soc.*, **87**, 104–109 (1965).
(25) F. K. Fong, *J. Am. Chem. Soc.*, **97**, 6890–6892 (1975).

Energy Dependence of the Radiationless Deactivation Rate for the Azulene System Probed by the Effect of External High Pressure

Dean J. Mitchell, Harry G. Drickamer,* and Gary B. Schuster*

Contribution from the School of Chemical Sciences and the Materials Research Laboratory, University of Illinois, Urbana, Illinois 61801. *Received April 7, 1977*

Abstract: The pressure dependence of the fluorescence of azulene and several of its derivatives was studied over a 130-kbar range. The efficiency of fluorescence from both the second and first excited singlet states was pressure dependent as was the relative energy of these states. It was shown that the fluorescence efficiency is limited by internal conversion from both excited singlets states. Furthermore, the rate of internal conversion was observed to depend strongly on the energy separating the relevant states.

Interest in the behavior of electronically excited azulene systems has been focused mainly on the rates of nonradiative decay from the excited singlet states of these molecules. Two unusual aspects of the radiationless decay from this chromophore have been noted. First, the second excited singlet state (S_2) of azulene fluoresces with a quantum efficiency of 0.02.[1] This unusually efficient anomalous fluorescence has been attributed to, among other things, inefficient competitive internal conversion to the first excited singlet state (S_1). Second, S_1 of azulene is essentially completely nonemissive. Fluorescence from this state has only recently been detected through the application of high-powered laser excitation.[2] Furthermore, the lifetime of S_1 has been measured by several different picosecond techniques. Although the exact magnitude of the S_1 lifetime varies depending upon the measuring procedure, it is clear that it is less than ca. 5 ps.[3] The rapid nonradiative relaxation of S_1 has been attributed to either internal conversion, intersystem crossing, or some combination of these two deactivation pathways.[4]

The application of external high pressure to the investigation of electronically excited molecules can reveal much about the pathways interconnecting the various states.[5] We have shown that the effect of application of external pressure to organic systems can be interpreted in terms of the interactions between the states of the molecule and the environment. Pressure can be used to probe the active decay modes of an electronically excited substance. We have shown that pressure-dependent behavior can be analyzed by a configuration coordinate model in which changes in vibrational force constants, relative potential energy, and position on the relevant intermolecular configuration parameter explain pressure-dependent behavior.[6] Moreover, in suitable systems it has proven possible to isolate these three parameters and analyze the pressure-dependent behavior of each.

In this paper we report our study of the pressure dependence of the emission and absorption for azulene and several of its derivatives. Primarily, the relationship between the relative energetic separation of the singlet states of these compounds and the efficiency of various energy degradation routes is probed. In addition, phosphorescence from suitably substituted azulenes permits further evaluation of the triplet state and the importance of competitive internal conversion and intersystem crossing from S_1.

Experimental Section

Azulene (**1**) (Aldrich) was purified by column chromatography (alumina) followed by recrystallization from methanol. Substituted azulenes **2**, **3**, **4**, and **6** were prepared by the procedure of Nozoe.[7] Bromo-substituted azulenes **5** and **7** were prepared using the procedure described by Eber.[8] All substituted azulenes were purified by chromatography and recrystallization before use.

Purification and polymerization of poly(methyl methacrylate) (PMMA) and polystyrene (PS) were described previously.[5] The compounds and plastic were dissolved in methylene chloride, forming approximately 0.05 M, 0.2 mm thick films after solvent evaporation. Emission was also investigated in solution of approximately 10^{-4} M.

The high-pressure cells and emission equipment, as well as methods of processing and analyzing the data, are described elsewhere.[9] The low-temperature techniques were developed by Tyner.[10] The transmission efficiency of the high-pressure cell for measurements below 40 kbar is independent of pressure. For the higher pressure range the transmission efficiency was calibrated using 9,10-diphenylanthracene (DPA) in PMMA, which has a fluorescence quantum yield near unity.[11] Above 100 kbar, however, the quantum yield of DPA appears